Cobalt@nitrogen-doped bamboo-structured carbon nanotube to boost photocatalytic hydrogen evolution on carbon nitride

Qiuxia Liu[a], Chunmei Zeng[a], Zhihui Xie[a], Lunhong Ai[a,b], Yaoyao Liu[a], Qin Zhou[a], Jing Jiang[a,b,*], Hongqi Sun[c], Shaobin Wang[b,d,*]

[a] Chemical Synthesis and Pollution Control Key Laboratory of Sichuan Province, College of Chemistry and Chemical Engineering, China West Normal University, Nanchong, 637002, China
[b] WA School of Mines: Minerals, Energy and Chemical Engineering, Curtin University, WA, 6102, Australia
[c] School of Engineering, Edith Cowan University, 270 Joondalup Drive, Joondalup, Perth, WA, 6027, Australia
[d] School of Chemical Engineering, The University of Adelaide, Adelaide, SA, 5005, Australia

A B S T R A C T

Rational design of high-efficiency and low-cost photo catalyst/cocatalyst systems is an effective strategy to realize high-performance photocatalytic hydrogen production from water, but remains still a great challenge. Herein, we report a new coatalyst based on ultra long bamboo-structured nitrogen-doped carbon nanotube (CNCNT) encapsulated with cobalt nanoparticles to couple with g-C_3N_4 photo catalyst in realizing a greatly enhanced photocatalytic activity toward hydrogen evolution reaction (HER). Taking advantages in effective electro catalytic HER activity, diversified spatial location and rapid interfacial charge transfer, the resulting g-C_3N_4/CNCNT exhibits significantly improved photocatalytic activity with a hydrogen evolution rate of 1208 $\mu mol\,g^{-1}\,h^{-1}$ in triethanolamine solution, achieving about 172-fold enhancement compared with pristine g-C_3N_4. More importantly, g-C_3N_4/CNCNT can photo catalytically decompose pure water with hydrogen evolution amount of about 92.3 $\mu mol\,g^{-1}$ within 4 h.

1. Introduction

Photocatalytic water splitting is an appealing sustainable approach toward transforming and storing solar light in the form of high energy density hydrogen fuel to meet the ever-increasing energy and environmental demands [1–3]. So far, intensive research efforts have been devoted to developing semiconductor photocatalysts for hydrogen evolution. However, most semiconductors bear the unsatisfactory hydrogen evolution activities and poor surface reaction rates, arising from the rapid recombination of the photo generated charge carriers other than for reaction. To overcome these limitations, engineering a co catalyst to combine with host photo catalysts would retard the recombination processes, since the co catalyst can promote the separation and migration of photo carriers and accommodate more reactive sites [4–9]. Typically, noble metal Pt is a widely used co catalyst to boost photocatalytic hydrogen evolution reaction [10,11]. However, practical large-scale applications are severely limited by its natural scarcity and high price. Therefore, it is important and especially valuable to explore low-cost and earth-abundant alternatives to facilitate highly efficient photocatalytic hydrogen evolution.

Up to now, various transition metal candidates, such as non-noble metals [12,13], sulfides [14–18], phosphides [19,20], carbides [21,22], nitrides [23,24], and hydroxides [25], have been explored as robust cocatalysts for promoting photocatalytic hydrogen evolution. Recent research eff;orts have also been made to understand the eff;ects of the cocatalyst size, morphology and location on the photo reactivity [26–29]. To further optimize photo catalysts, complex multicomponent cocatalysts are designed and fabricated to precisely control charge spatial location of the photocatalytic systems, which are difficult to achieve in a single-component co catalyst. To meet the favourable energy synergy, it usually requires strong bonding and large contact interface between different components in multicomponent co catalyst systems [29,30]. Fortunately, the multicomponent nanocarbon-based materials provide an ideal platform to achieve this goal. For instance, synergistic MoS_2/graphene co catalyst with an intimate contact between MoS_2 and graphene achieves significantly higher co catalytic activities on host photo catalysts (e.g. TiO_2 [31], CdS [32] and g-C_3N_4 [33]) than single-component MoS_2 and pristine graphene. Likewise,

---

* Corresponding authors at: Chemical Synthesis and Pollution Control Key Laboratory of Sichuan Province, College of Chemistry and Chemical Engineering, China West Normal University, Nanchong 637002, China.
E-mail addresses: 0826zjjh@163.com (J. Jiang), shaobin.wang@adelaide.edu.au (S. Wang).

different Ni@nanocarbon co catalysts including Ni@graphene [34], nanoconfined Ni@C [30] and single nickel atoms on nitrogen-doped graphene (Ni-NG) [35] have been demonstrated to greatly enhance the photocatalytic activities of various semiconductor photocatalysts. Moreover, other types of nanocarbon-based multicomponent co catalysts such as $Ni_2P/Ni@C$ [36], Cu_3P-carbon nanotube [37], and $Mo_2C@C$ [38,39] were also loaded on host photocatalysts to significantly improve the photocatalytic activity for hydrogen evolution. Despite these advances, the catalyst performances are still far away from the satisfaction due to the discontinuous interface and limited contact area in spatial location. Therefore, creating a new class of interfacial co catalyst materials via engineering spatial contact is still a great challenge.

Bearing above issues in mind, we herein explore ultra long bamboo-structured nitrogen-doped carbon nanotube encapsulating cobalt nanoparticles (CNCNT) as a new co catalyst to synergistically combine with host photo catalyst based on the following considerations. (i) CNCNT would work as an electron donor to accept the electrons photo excited from the host photo catalyst to retard the recombination of photo generated charge carriers; (ii) CNCNT possesses intrinsic electrocatalytic activity due to its excellent electron penetration and transport characteristics [40,41]. Electron injection process from a host photo catalyst to CNCNT resembles the physical process that the applied electric field in electro catalysis for CNCNT, and the proton reduction step involved in CNCNT co catalyst for photo catalysis would be similar to that occurred on the surface of CNCNT as an electro catalyst; (iii) CNCNT with a unique structure could favorably expand spatial scale and enrich reaction sites, ensuring the smooth electron flow to achieve the maximization of electron utilization efficiency. Subsequently, we develop a facile and inexpensive approach to construct g-C_3N_4/CNCNT systems by only using melamine as carbon and nitrogen sources, and elucidate the CNCNT co catalyst effect on the photocatalytic process of the g-C_3N_4/CNCNT. As a result, the optimal g-C_3N_4/CNCNT exhibits significantly enhanced photocatalytic activity with H_2 evolution rate of 1208 $\mu mol\,g^{-1}\,h^{-1}$ in the presence of triethanolamine (TEOA), which is nearly 172 times higher than that of pure g-C_3N_4 and even superior to most of the previously reported g-C_3N_4/co catalyst systems under similar conditions. More importantly, g-C_3N_4/CNCNT shows a strong ability to photo

catalytically decompose pure water and affords a comparable H_2 evolution amount of about 92.3 $\mu mol\,g^{-1}$ within 4 h.

2. Experimental

2.1. Materials

$CoCl_2\cdot6H_2O$, melamine, triethanolamine (TEOA), and Na_2SO_4 were purchased from Chengdu Kelong Chemical Reagents Company and used as received without further purification.

2.2. Synthesis of bamboo-like Co@NCNT

The bamboo-like Co@NCNT (CNCNT) was synthesized according to our previous report with some modifications [42]. Briefly, 4 mmol of $CoCl_2\cdot6H_2O$ and 16 mmol of melamine are uniformly mixed by mechanical grinding and then calcined at 700 °C for 1.5 h under nitrogen atmosphere with a ramp rate of 10 °C min^{-1}. The as-annealed products were soaked in a 3 M HCl solution overnight, rinsed with distilled water and dried in an oven at 60 °C.

2.3. Synthesis of g-C_3N_4/CNCNT

Typically, 50 mmol of melamine was put into a porcelain crucible with a cover and then calcined at 550 °C for 2 h in a muffle furnace with a heating rate of 5 °C min^{-1}. The pristine g-C_3N_4 was obtained after cooling to room temperature. Next, certain amounts of g-C_3N_4 and

CNCNT were separately suspended in distilled water and sonicated for two days. The dispersions were centrifuged at 6000 rpm for 10 min to remove aggregates. Then, g-C_3N_4 and CNCNT dispersions at different ratios were mixed and sonicated for another two days. After drying at 80 °C for 24 h, products of g-C_3N_4/CNCNT were obtained (Table S1, Supporting information). Among all the products, g-C_3N_4/CNCNT-3:2 presents the best photocatalytic activity; therefore, if no further indication, the g-C_3N_4/CNCNT notation in this study refers to g-C_3N_4/CNCNT-3:2.

2.4. Characterization

Powder X-ray diffraction (XRD) measurements were acquired on a Rigaku Dmax/Ultima IV diffractometer equipped with a monochromatized Cu Kα source. The morphologies and elemental mapping were determined by a Hitachi S4800 scanning electron microscope and a FEI Tecnai G 20 transmission electron microscope (TEM). X-ray photoelectron spectroscopy (XPS) was taken on a Perkin-Elmer PHI 5000C instrument using a monochromatic Al Kα. Fourier transform infrared (FTIR) spectra were recorded on a Nicolet 6700 spectrometer. UV–vis diffuse reflectance spectra were measured with a Shimadzu UV-3600 spectrophotometer. Nitrogen adsorption-desorption isotherms were performed on a Quantachrome ASIQ-C apparatus at −196 °C. Photoluminescence (PL) spectroscopy was collected on a Cary Eclipse fluorescence spectrometer. Time-resolved fluorescence spectroscopy was recorded on a Edinburgh FLS920 spectrophotometer.

2.5. Electrochemical measurements

For the preparation of a working electrode, 2 mg of catalyst powders were homogeneously mixed with 2 mL of ethanol and 60 μL of Nafion (5 wt%) for a disersed solution. The dispersion (100 μL) was then drop-casted onto an indium-tin oxide (ITO) glass electrode with a coated area of ~1 cm^2. Transient photocurrent measurements and electrochemical impedance spectroscopy (EIS) were performed on a CHI660E electrochemical workstation in a typical three-electrode setup with an electrolyte solution of 0.5 M Na_2SO_4, using Pt foil as the counter electrode, an Ag/AgCl electrode as the reference electrode and the modified ITO glass as the working electrode.

For electro catalytic HER, 5 mg of catalyst powders were homogeneously mixed with 1 mL of water-ethanol (3:1 v/v) solution and 5 μL of Nafion (5 wt%) under sonication at least 30 min. The dispersion (5 μL) was then drop-casted onto the glassy carbon electrode with the diameter of 3 mm. The electrochemical HER experiments were performed in a similar typical three-electrode setup with an electrolyte solution of 0.5 M H_2SO_4 using a modified glassy carbon electrode as the working electrode. All potentials measured were converted to the reversible hydrogen electrode (RHE) scale according to the Nernst equation: $E_{RHE} = E_{Ag/AgCl} + 0.197\,V + 0.059\,pH$.

2.6. Photocatalytic activity evaluation

The photocatalytic hydrogen evolution experiments were carried out in an online photocatalytic test system (Au Light, CEL-SPH2N system, Beijing) at ambient temperature. A photo catalyst (20 mg) was suspended in a 20 mL 10% TEOA aqueous solution (or 20 mL water without any sacrificial agent) under continuously magnetic stirring. The photocatalytic reaction system was thoroughly degassed and irradiated by a 300 W Xe lamp with a light intensity of 148.2 mW cm^{-2}. The evolved H_2 was monitored periodically by an online gas chromatograph with a thermal conductivity detector.

3. Results and discussion

Bamboo-structured CNCNT is synthesized by a one-step solid-state reaction approach and the fabrication of CNCNT is schematically
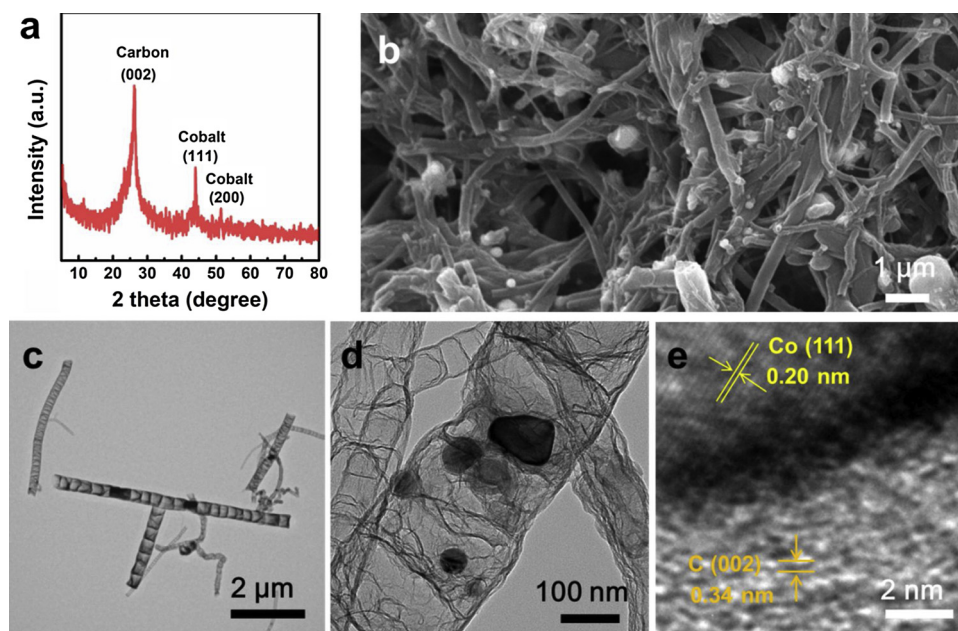
Fig. 1. XRD pattern (a), SEM (b), TEM (c,d) and HRTEM (e) images of CNCNT.

illustrated in Fig. S1. The X-ray diffraction (XRD) pattern displayed in Fig. 1a reveals the CNCNT is comprised of two phase structures of graphitic carbon and face centered cubic (fcc) cobalt. A general scanning electron microscopy (SEM) image (Fig. 1b) confirms the high yield of the carbon nanotubes with uniform diameters, ultralong and flexible structures. The typical transmission electron microscopy (TEM) image (Fig. 1c) further discloses the carbon nanotubes in a bamboo-like structure, in which some nanosized particles sparsely distributed inside the nanotubes (Fig. 1d). A corresponding high-resolution TEM image (HRTEM, Fig. 1e) illustrates the distinct lattice fringes with d-spacing of 0.34 and 0.20 nm, which are in good agreement with the (002) and (111) planes of graphitic carbon and metallic Co, respectively. To explore the potential of CNCNT as an effective co catalyst, we further evaluate its capability toward electro catalytic HER. Fig. S2 shows the polarization curves of the CNCNT at a scan rate of $5 \, mV \, s^{-1}$ in 0.5 M H_2SO_4 solution. The CNCNT is capable toward electro catalytic HER evidenced by the relatively small HER over potential, confirming its good electro catalytic HER activity [43,44].

Graphitic carbon nitride (g-C_3N_4) possesses a framework topology in the form of two-dimension nano sheets. Moreover, when a certain proportion of g-C_3N_4 disperses into water solution, it can stabilize as uniformly processable aqueous dispersion [45–47], providing the favorable merits to be integrated with other materials. To this end, we developed a solution strategy to couple g-C_3N_4 with CNCNT in a self-assembly. As shown in Fig. 2a, the optimized g-C_3N_4/CNCNT solution is relatively stable after two days ultrasonic self-assembly and even retains good stability at least one month, which is beneficial from the conjugation interaction between 2D planar structures of g-C_3N_4 and 1D carbon nanotubes of CNCNT. Moreover, the ultra long CNCNT as a bridge to interact small carbon nitride nano sheets can form the interconnected network promoting the structural stability.

Fig. 2b shows the XRD patterns of the as-prepared g-C_3N_4/CNCNT. Pristine g-C_3N_4 exhibits two distinct diffraction peaks at 13.2° (100) and 27.8° (002), corresponding to the in-planar ordering of the heptazine units and the characteristic stacking of the conjugated aromatic structure, respectively [48–51]. Apart from the characteristic diffraction peaks of g-C_3N_4, a broad peak centered at 26.1° indexed as the (002) reflection of carbon nanotubes and a weak peak at 44.0° assigned to the (111) reflection of metallic Co are also observed in the XRD patterns of g-C_3N_4/CNCNT, which become more visible at the relative

large content of CNCNT in g-C_3N_4/CNCNT. As shown in Fig. 2c, the structures of g-C_3N_4/CNCNT were also confirmed by FTIR spectroscopy. The g-C_3N_4/CNCNT displays almost the identical spectra to that of pristine g-C_3N_4. Specifically, a broad peak in the range of 3000-3500 cm^{-1} is attributed to the stretching vibration mode of N-H, while the peaks between 1100 and 1700 cm^{-1} are associated with the stretching vibration modes of aromatic C-N heterocycles [11,52]. The characteristic peak at 814 cm^{-1} is attributed to the stretching vibration mode of the triazine subunits. The optical properties of g-C_3N_4/CNCNT were further determined by UV-vis diffuse reflectance spectroscopy (DRS). As shown in Fig. 2d, the light absorption edge of pristine g-C_3N_4 is at about 460 nm, which corresponds to a band gap (E_g) of ~2.69 eV and is consistent with previously reported results [53,54], whereas the CNCNT presents a flat plot with an intensive absorption in the wavelength range. With regard to g-C_3N_4/CNCNT, there is no obvious shift in light absorption edges, but the absorption intensity is significantly enhanced at the wavelength region above 450 nm. These observations indicate the effective combination of g-C_3N_4 and CNCNT to form the g-C_3N_4/CNCNT.

The microstructure and morphology of g-C_3N_4/CNCNT were further investigated by TEM. A typical TEM image (Fig. 3a) reveals 2D nanosheets and porous textures of the pristine g-C_3N_4. Fig. 3b is a general TEM image of the g-C_3N_4/CNCNT, which clearly manifests that the sample is composed of both sheet-like g-C_3N_4 and bamboo-like CNCNT, bearing rather intimate contacts with each other on different spatial locations. Some CNCNT freely stands (Fig. 3b) while the others closely lie on the g-C_3N_4 nano sheets (Fig. 3c). The ultra long conductive CNCNT acts as a bridge in connection with lots of g-C_3N_4 nano sheets (Fig. 3d). This structural feature supplies an electron highway, guaranteeing rapid charge transportation efficiency during photo catalysis. In addition, high-angle annular dark-field scanning TEM (HAADF-STEM) image and corresponding elemental mapping (Fig. 3e) confirm the g-C_3N_4/CNCNT is composed of C, N, and Co in uniform distributions.

The chemical state and elemental composition of g-C_3N_4/CNCNT were further analyzed by X-ray photoelectron spectroscopy (XPS). As shown in Fig. 4a, the survey spectrum suggests the coexistence of C, N and Co elements in the product. Fig. 4b shows the high-resolution XPS spectrum of C 1 s, which can be deconvoluted into three peaks at binding energies (BEs) of 284.6 eV (C-C), 285.3 eV (C−N) and 288.7 eV
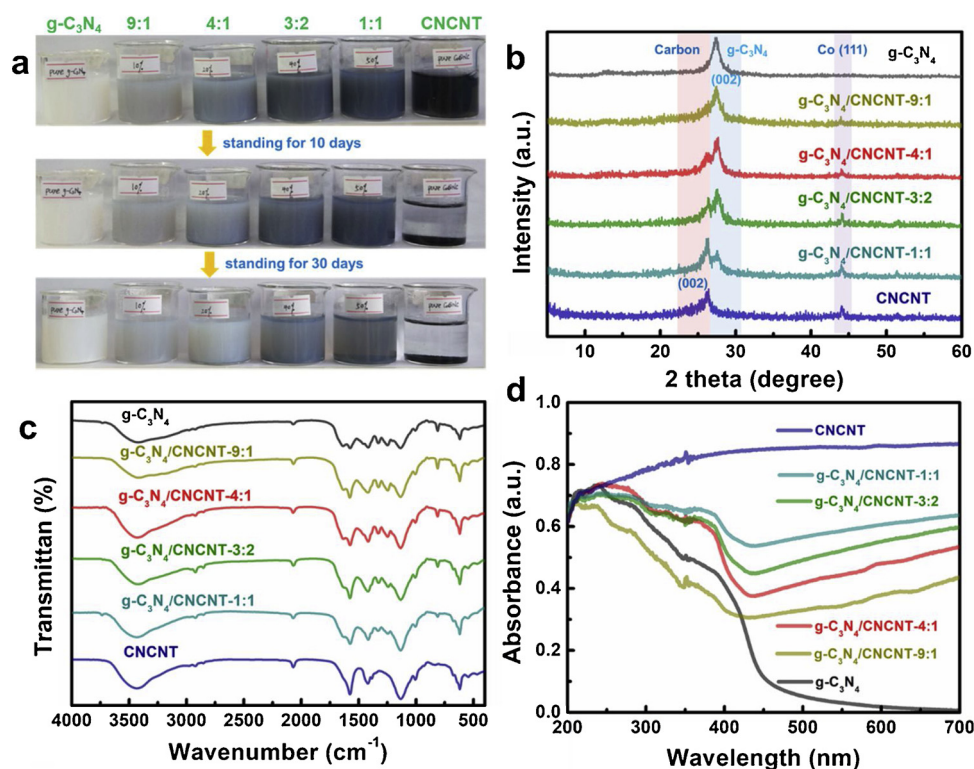
Fig. 2. (a) Digital photos of g-C$_3$N$_4$, CNCNT and g-C$_3$N$_4$/CNCNT aqueous dispersions. (b) XRD patterns, (c) FTIR spectra and (d) UV-vis DRS of g-C$_3$N$_4$, CNCNT and g-C$_3$N$_4$/CNCNT.

(N−C = N) in g-C$_3$N$_4$/CNCNT [55]. The high-resolution XPS spectrum of N 1 s (Fig. 4c) can be deconvoluted into three peaks at 398.7, 399.4 and 401.2 eV, which are attributed to C−N = C, N-C$_3$ and N−H in g-C$_3$N$_4$/CNCNT, respectively [56]. The high-resolution Co 2p XPS spectrum (Fig. 4d) exhibits a relatively weak intensity, implying a low content of Co species in g-C$_3$N$_4$/CNCNT. More specifically, the peaks located at BEs of 778.5 and 794.2 eV are ascribed to Co°, whereas other peaks at BEs of 781.6 and 797.5 eV are assigned to Co−O from the surface oxidized Co species [57].

The photocatalytic hydrogen evolution performances of the g-C$_3$N$_4$/

CNCNT were tested in the presence of TEOA as a hole acceptor without the use of any noble-metal-based co catalysts. As shown in Fig. 5a, pristine g-C$_3$N$_4$ presents a negligible activity with a rather low hydrogen generation amount of 26 µmol g^{-1} after 4 h of irradiation, arising from its rapid charge recombination and small specific surface area (Fig. S3, Supporting information). In a sharp contrast, the hydrogen evolution activity is apparently enhanced after the combination of CNCNT with g-C$_3$N$_4$. More specifically, g-C$_3$N$_4$/CNCNT-3:2 exhibits the best photocatalytic activity with H$_2$ evolution amount of around 4917 µmol g^{-1}. As plotted in Fig. 5b, the H$_2$ generation rate of the g-
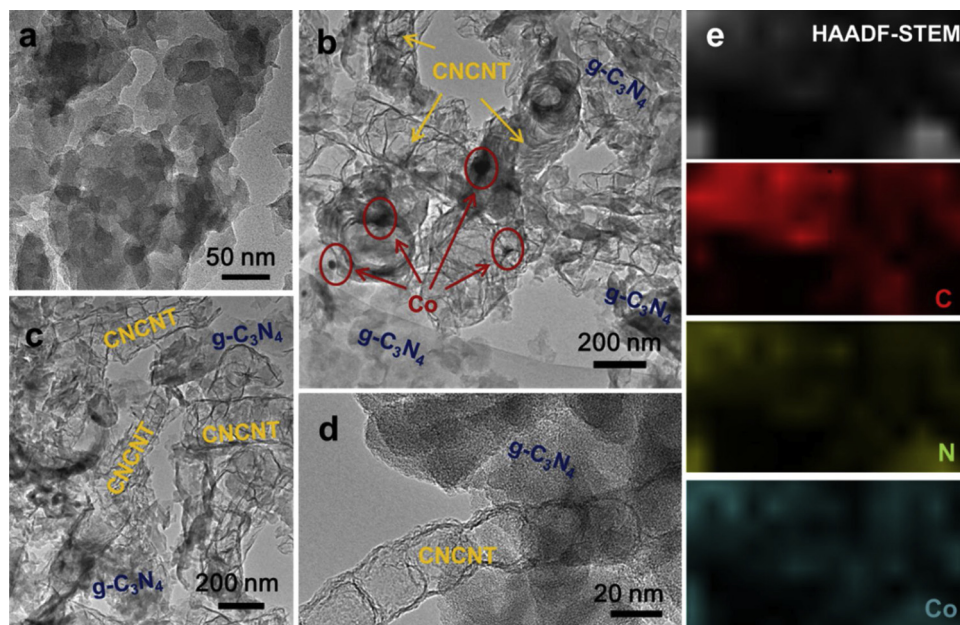

Fig. 3. (a) TEM image of g-C$_3$N$_4$. (b-d) TEM images and (e) HAADF-STEM elemental mapping images of g-C$_3$N$_4$/CNCNT.
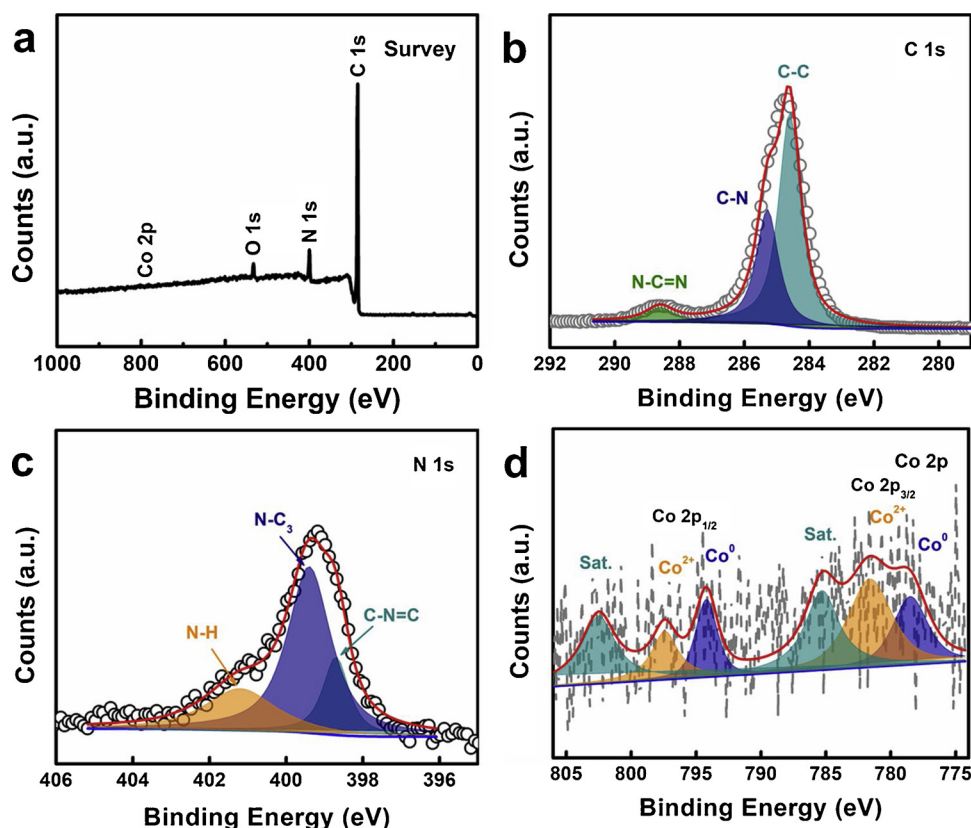
Fig. 4. XPS spectra of g-C$_3$N$_4$/CNCNT: (a) Survey, (b) C 1 s, (c) N 1 s, (d) Co 2p.
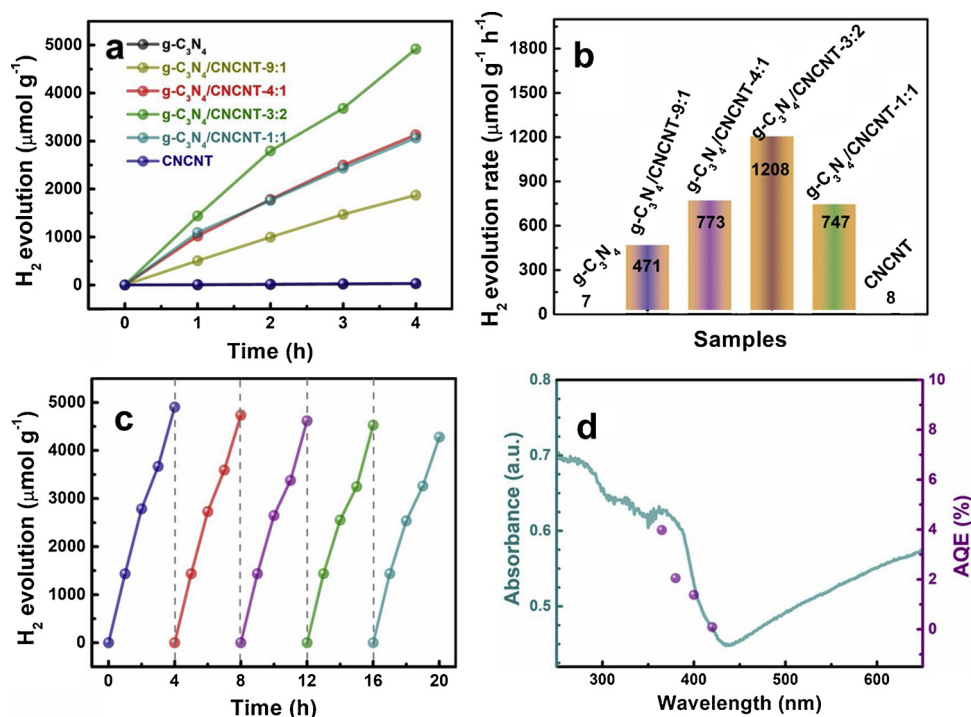

Fig. 5. Photocatalytic hydrogen production of different photocatalysts: (a) hydrogen production against time and (b) hydrogen production rate. (c) Reusability tests of g-C$_3$N$_4$/CNCNT for photocatalytic H$_2$ evolution. (d) Quantum efficiency of g-C$_3$N$_4$/CNCNT at different wavelengths.

C$_3$N$_4$/CNCNT-3:2 is about 1208 μmol g^{-1} h^{-1}, which is nearly 172 times higher than those of pure g-C$_3$N$_4$ and CNCNT, and is 2.56, 1.56, and 1.62 times as high as those of g-C$_3$N$_4$/CNCNT-9:1, g-C$_3$N$_4$/CNCNT-4:1, and g-C$_3$N$_4$/CNCNT-1:1, respectively. Such performance

outperforms most of the cocatalyst modified g-C$_3$N$_4$-based photocatalysts reported previously for hydrogen generation (Table S2, Supporting information), such as MoS$_2$ (576.6 μmol g^{-1} h^{-1}) [58], CoP (1125 μmol g^{-1} h^{-1}) [59], NiB (464.4 μmol g^{-1} h^{-1}) [60], NiS

Fig. 6. (a) PL spectra of g-C_3N_4 and g-C_3N_4/CNCNT. Time-resolved transient PL decay curves of (b) g-C_3N_4 and (c) g-C_3N_4/CNCNT. (d) Transient photocurrent responses, (e) Nyquist plots, (f) HER polarization curves of g-C_3N_4 and g-C_3N_4/CNCNT.

(366.4 $\mu mol\,g^{-1}\,h^{-1}$) [61], Ti_2C (950 $\mu mol\,g^{-1}\,h^{-1}$) [62], polypyrrole (154 $\mu mol\,g^{-1}\,h^{-1}$) [63], $CoTiO_3$ (858 $\mu mol\,g^{-1}\,h^{-1}$) [64], PtAu (1009 $\mu mol\,g^{-1}\,h^{-1}$) [65], and Pt nanoparticle (813.3 $\mu mol\,g^{-1}\,h^{-1}$) [66]. The stability of photocatalytic H_2 generation over g-C_3N_4/CNCNT was further evaluated by cycling experiments. As shown in Fig. 5c, the g-C_3N_4/CNCNT nearly maintains the original hydrogen evolution activity in five cycles for 20 h, revealing good stability of the g-C_3N_4/CNCNT for photocatalysis. The apparent quantum efficiency (AQE) of the g-C_3N_4/CNCNT under various incident monochromatic light was also measured. As displayed in Fig. 5d, the g-C_3N_4/CNCNT exhibits the AQE of 3.98%, 2.05%, 1.38% and 0.09% at 365, 380, 400 and 420 nm, respectively.

The photo physical properties of charge carriers in light-excited photo catalysts mainly dominate the underlying photocatalytic activities [67–69]. We therefore conduct a series of the related spectroscopic and photoelectrochemical tests to probe the behaviors of the photo generated charge carriers. The trapping and recombination of photo induced electron-hole pairs on the surface of photo catalyst could be reflected by steady state photoluminescence (PL) spectroscopy. Fig. 6a presents the steady state PL spectra of pure g-C_3N_4 and g-C_3N_4/CNCNT. The PL peak intensity of the g-C_3N_4/CNCNT at approximately 450 nm is dramatically decreased in comparison with g-C_3N_4, elucidating that CNCNT facilitates the charge separation and migration, further effectively retarding the recombination of the photoinduced electron-hole pairs in g-C_3N_4. The time-resolved PL transient decay spectroscopy validates the improved charge separation efficiency as well. As shown in Fig. 6b and Fig. 6c, the g-C_3N_4/CNCNT exhibits an obviously slower exponential decay based on the tri-exponential function fitting (Table S3, Supporting information). The estimated average lifetime of the g-C_3N_4/CNCNT (32.53 ns) is distinctly prolonged as compared to that of g-C_3N_4 (7.53 ns). The observed long carrier lifetime suggests that CNCNT functions as both a bridge to assist the charge separation and a channel to promote charge transport, which are beneficial to boosting photocatalytic performance. The improved performance of photo-induced charge carriers is also confirmed by the transient photocurrent responses and electrochemical impedance spectroscopy (EIS). As displayed in Fig. 6d, both the g-C_3N_4 and the g-C_3N_4/CNCNT exhibit rapid photocurrent responses under intermittent illumination, which are stable and can be well repeated in several on-off cycles. More specifically, the photocurrent density produced by g-C_3N_4/CNCNT is about 3.59 $\mu A\,cm^{-2}$, which is three times as high as that of g-C_3N_4 ($^\sim$1.16 $\mu A\,cm^{-2}$), demonstrating that the improved separation

efficiency of the photoinduced electron-hole pairs in the g-C_3N_4/CNCNT. A similar tendency was also observed in EIS (Fig. 6e), where the semicircular arc diameter of g-C_3N_4/CNCNT is much smaller than that of bare g-C_3N_4, further clarifying the greatly enhanced charge migration efficiency owing to the shortened migration distance arising from the bridge-effect induced interfacial interaction between g-C_3N_4 and CNCNT. On the basis of these results, it can be inferred that the more effective charge separation and faster interfacial charge transport are responsible for the boosted photocatalytic performance.

In addition to the charge carrier behavior in g-C_3N_4 affected by CNCNT, we hypothesize the energy efficiency of CNCNT cocatalyst for photocatalytic hydrogen evolution would be related to its electro-catalytic performance for water reduction. The electrocatalytic HER performances of pure g-C_3N_4 and g-C_3N_4/CNCNT were further studied (Fig. 6f). The pure g-C_3N_4 is totally inactive for electrocatalytic hydrogen evolution, while the incorporation of CNCNT leads to the obvious electrocatalytic HER activity and favorable HER kinetics of g-C_3N_4/CNCNT, coincidence with the tendency in the above EIS results. Inspiring that electron injection from g-C_3N_4 to CNCNT in photo catalysis is analogous to the applied electric field for CNCNT during the electro catalysis (Fig. 7a), we assume the HER-active g-C_3N_4/CNCNT would be still active for photo catalytically decomposing pure water without any sacrificial agent. Surprisingly, molecular hydrogen could be evolved from pure water over g-C_3N_4/CNCNT, giving hydrogen at about 92.3 $\mu mol\,g^{-1}$ within 4 h of irradiation (Fig. 7b). The initial induction period in first one hour could be attributed to the absence of hole scavenger, resulting in the slow surface reaction kinetics, which is also encountered in previously reported photocatalytic systems for water splitting [70–72].

To further gain insight into the charge behavior, the band structures of g-C_3N_4 and CNCNT were investigated by ultraviolet photoelectron spectroscopy (UPS) with a monochromatic HeI light source (21.2 eV). According to the linear extrapolation method [73,74], the work function (Φ) can be calculated according to the equation: $\Phi = 21.2 - E_{onset}$, where E_{onset} is the secondary electron cut off edge (Fig. 8a and 8c), while the valence band potential (E_{VB}) in vacuum level is obtained by the sum of Φ and VB edge (Fig. 8b). Thus, the E_{VB} for g-C_3N_4 is estimated to be 1.92 eV below Fermi level (E_F), while the Φ values for g-C_3N_4 and CNCNT are 4.3 and 5.24 eV, respectively. By combination of the bandgap estimated from DRS, the conduction band potential (E_{CB}) of the g-C_3N_4 in vacuum level is determined to be 0.77 eV above E_F. The energy band diagram of g-C_3N_4 and CNCNT versus with respect to
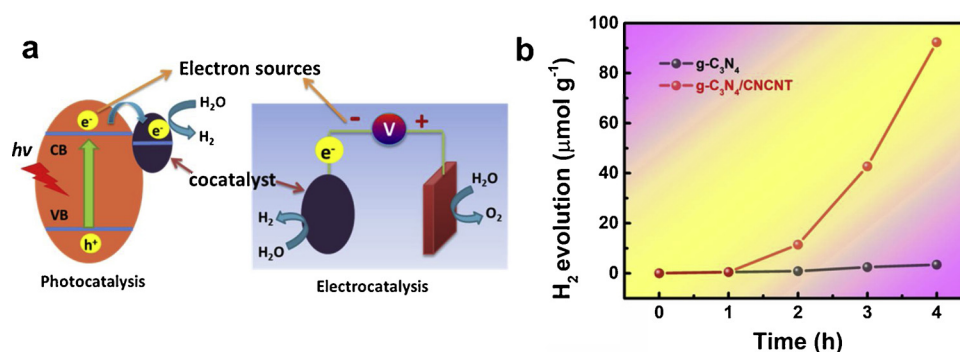
Fig. 7. (a) Schematic illustration of the relationship between photocatalysis and electrocatalysis for electrocatalytically active cocatalyst. (b) Photocatalytic hydrogen production in pure water of g-C_3N_4 and g-C_3N_4/CNCNT.

vacuum level is depicted in Fig. 8d. On the basis of above analyses, a plausible photocatalytic mechanism of g-C_3N_4/CNCNT is proposed and illustrated in Fig. 8e. The g-C_3N_4 with a favorable bandgap can interact with light to produce photo induced electron-hole pairs. However, these photo carriers within photo excited g-C_3N_4 rapidly recombine in the absence of any cocatalyst, resulting in a poor photo reactivity. By the combination of CNCNT, the difference in the work function between g-C_3N_4 and CNCNT creates rapid charge carrier transfer to intrinsically steer the spatial separation of photo excited electron-hole pairs, which is similar to that of MoS_2 co catalyst [16,75–77]. Moreover, the bridge-
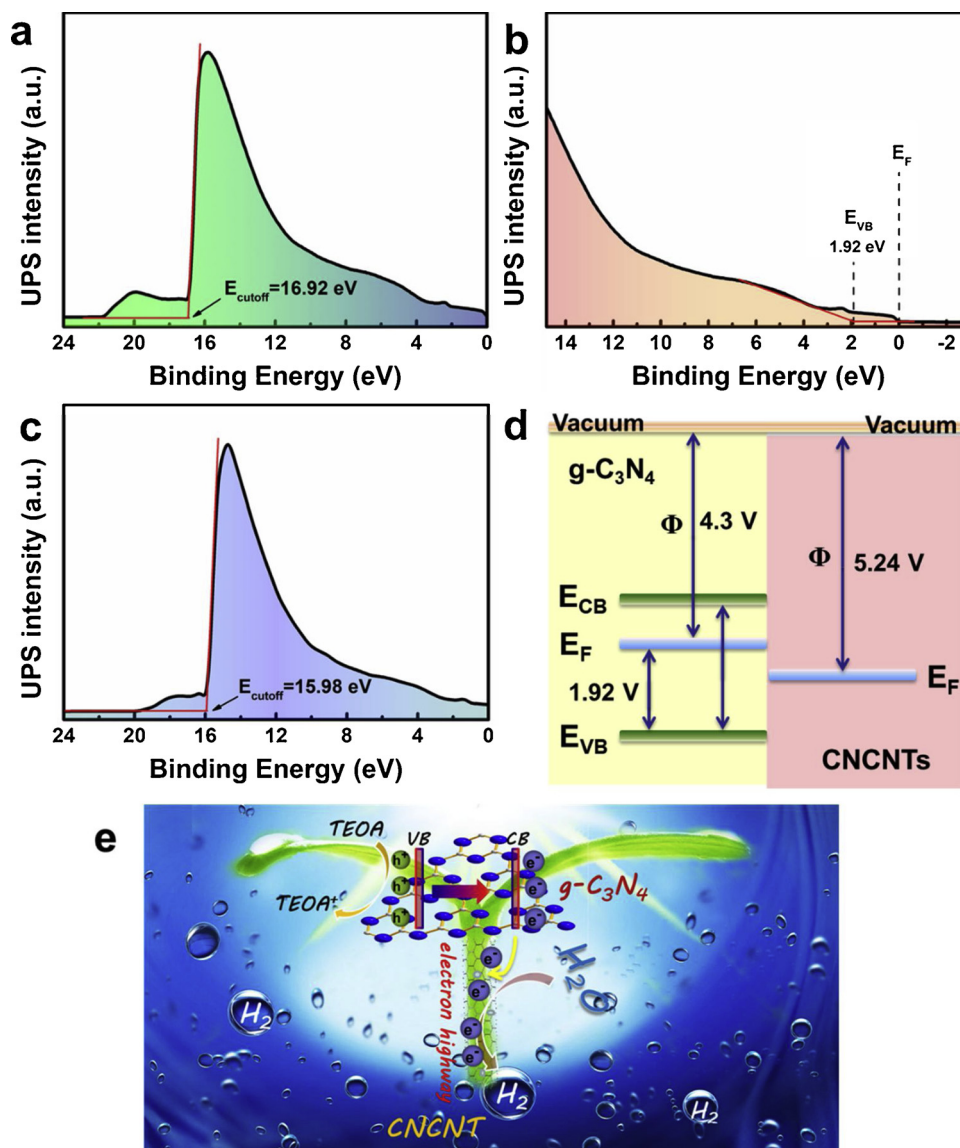

Fig. 8. UPS spectrum of g-C_3N_4: (a) onset level of secondary electron cutoff and (b) near the Fermi level energy and valence band maximum. (c) Onset level of secondary electron cutoff of UPS spectrum of CNCNT. (d) Band alignment of g-C_3N_4 and CNCNT. (e) Photocatalytic mechanism of g-C_3N_4/CNCNT.

effect induces interfacial interaction between g-C$_3$N$_4$ and CNCNT and electrocatalytically active nature of CNCNT will further optimize the charge carrier behavior to reduce transfer barrier and promote the reactive efficiency of photo carriers.

4. Conclusions

In summary, we have successfully constructed a photo catalyst/co catalyst system of g-C$_3$N$_4$/CNCNT by a facile and inexpensive method, where the ultra long CNCNT cocatalyst is synergistically coupled with a host g-C$_3$N$_4$ photo catalyst. Benefiting from the intrinsic electro catalytic HER activity, diversified spatial location and accelerated interfacial charge transfer, the g-C$_3$N$_4$/CNCNT shows remarkably improved photocatalytic activity, achieving hydrogen evolution rate of nearly 172 times as high as that of pure g-C$_3$N$_4$. More importantly, g-C$_3$N$_4$/CNCNT can photo catalytically split pure water with comparable hydrogen evolution amount. This study suggests that the electro catalytic CNCNT could be a promising cocatalyst to efficiently boost photocatalytic water splitting.

Acknowledgements

Appendix A. Supplementary data

Supplementary material related to this article can be found, in the online version, at doi:https://doi.org/10.1016/j.apcatb.2019.04.098.

References

[1] A. Fujishima, K. Honda, Electrochemical photolysis of water at a semiconductor electrode, Nature 238 (1972) 37–38.

[2] X. Chen, S. Shen, L. Guo, S.S. Mao, Semiconductor-based photocatalytic hydrogen generation, Chem. Rev. 110 (2010) 6503–6570.

[3] T. Hisatomi, J. Kubota, K. Domen, Recent advances in semiconductors for photocatalytic and photoelectrochemical water splitting, Chem. Soc. Rev. 43 (2014) 7520–7535.

[4] J. Yang, D. Wang, H. Han, C. Li, Roles of cocatalysts in photocatalysis and photoelectrocatalysis, Acc. Chem. Res. 46 (2013) 1900–1909.

[5] K. Maeda, K. Domen, Photocatalytic water splitting: recent progress and future challenges, J. Phys. Chem. Lett. 1 (2010) 2655–2661.

[6] Z. Qin, Y. Chen, X. Wang, X. Guo, L. Guo, Intergrowth of cocatalysts with host photocatalysts for improved solar-to-hydrogen conversion, ACS Appl. Mater. Interfaces 8 (2016) 1264–1272.

[7] W. Bi, L. Zhang, Z. Sun, X. Li, T. Jin, X. Wu, Q. Zhang, Y. Luo, C. Wu, Y. Xie, Insight into electrocatalysts as co-catalysts in efficient photocatalytic hydrogen evolution, ACS Catal. 6 (2016) 4253–4257.

[8] D. Huang, Z. Li, G. Zeng, C. Zhou, W. Xue, X. Gong, X. Yan, S. Chen, W. Wang, M. Cheng, Megamerger in photocatalytic field: 2D g-C$_3$N$_4$ nanosheets serve as support of 0D nanomaterials for improving photocatalytic performance, Appl. Catal. B: Environ. 240 (2018) 153–173.

[9] J. Ran, J. Zhang, J. Yu, M. Jaroniec, S.Z. Qiao, Earth-abundant cocatalysts for semiconductor-based photocatalytic water splitting, Chem. Soc. Rev. 43 (2014) 7787–7812.

[10] Q. Li, B. Guo, J. Yu, J. Ran, B. Zhang, H. Yan, J.R. Gong, Highly efficient visible-light-driven photocatalytic hydrogen production of CdS-cluster-decorated graphene nanosheets, J. Am. Chem. Soc. 133 (2011) 10878–10884.

[11] J. Zhang, M. Zhang, C. Yang, X. Wang, Nanospherical carbon nitride frameworks with sharp edges accelerating charge collection and separation at a soft photocatalytic interface, Adv. Mater. 26 (2014) 4121–4126.

[12] P.D. Tran, L. Xi, S.K. Batabyal, L.H. Wong, J. Barber, J.S.C. Loo, Enhancing the photocatalytic efficiency of TiO$_2$ nanopowders for H$_2$ production by using non-noble transition metal co-catalysts, Phys. Chem. Chem. Phys. 14 (2012) 11596–11599.

[13] S. Xiao, P. Liu, W. Zhu, G. Li, D. Zhang, H. Li, Copper nanowires: a substitute for noble metals to enhance photocatalytic H$_2$ generation, Nano Lett. 15 (2015) 4853–4858.

[14] X. Zong, H. Yan, G. Wu, G. Ma, F. Wen, L. Wang, C. Li, Enhancement of photocatalytic H$_2$ evolution on CdS by loading MoS$_2$ as cocatalyst under visible light irradiation, J. Am. Chem. Soc. 130 (2008) 7176–7177.

[15] Y. Hou, Y. Zhu, Y. Xu, X. Wang, Photocatalytic hydrogen production over carbon nitride loaded with WS$_2$ as cocatalyst under visible light, Appl. Catal. B: Environ. 156 (2014) 122–127.

[16] H. Xu, J. Yi, X. She, Q. Liu, L. Song, S. Chen, Y. Yang, Y. Song, R. Vajtai, J. Lou, 2D heterostructure comprised of metallic 1T-MoS$_2$/Monolayer O-g-C$_3$N$_4$ towards efficient photocatalytic hydrogen evolution, Appl. Catal. B: Environ. 220 (2018) 379–385.

[17] Y. Xia, S. Liang, L. Wu, X. Wang, Ultrasmall NiS decorated HNb$_3$O$_8$ nanosheeets as highly efficient photocatalyst for H$_2$ evolution reaction, Catal. Today 330 (2018) 195–202.

[18] Y. Liu, C. Zeng, L. Ai, J. Jiang, Boosting charge transfer and hydrogen evolution performance of CdS nanocrystals hybridized with MoS$_2$ nanosheets under visible light irradiation, Appl. Surf. Sci 484 (2019) 692–700.

[19] Z. Sun, H. Zheng, J. Li, P. Du, Extraordinarily efficient photocatalytic hydrogen evolution in water using semiconductor nanorods integrated with crystalline Ni$_2$P cocatalysts, Energy Environ. Sci. 8 (2015) 2668–2676.

[20] A. Indra, A. Acharjya, P.W. Menezes, C. Merschjann, D. Hollmann, M. Schwarze, M. Aktas, A. Friedrich, S. Lochbrunner, A. Thomas, Boosting visible-light-driven photocatalytic hydrogen evolution with an integrated nickel phosphide–carbon nitride system, Angew. Chem. Int. Ed. 56 (2017) 1653–1657.

[21] Y.-L. Men, Y. You, Y.-X. Pan, H. Gao, Y. Xia, D.-G. Cheng, J. Song, D.-X. Cui, N. Wu, Y. Li, Selective CO evolution from photoreduction of CO$_2$ on a metal-carbide-based composite catalyst, J. Am. Chem. Soc. 140 (2018) 13071–13077.

[22] A.T. Garcia-Esparza, D. Cha, Y. Ou, J. Kubota, K. Domen, K. Takanabe, Tungsten carbide nanoparticles as efficient cocatalysts for photocatalytic overall water splitting, ChemSusChem. 6 (2013) 168–181.

[23] H. Chen, D. Jiang, Z. Sun, R.M. Irfan, L. Zhang, P. Du, Cobalt nitride as an efficient cocatalyst on CdS nanorods for enhanced photocatalytic hydrogen production in water, Catal. Sci. Technol. 7 (2017) 1515–1522.

[24] N. Han, P. Liu, J. Jiang, L. Ai, Z. Shao, S. Liu, Recent advances in nanostructured metal nitrides for water splitting, J. Mater. Chem. A 6 (2018) 19912–19933.

[25] Y. Xia, W. Chen, S. Liang, J. Bi, L. Wu, X. Wang, Engineering a highly dispersed cocatalyst on a few-layered catalyst for efficient photocatalytic H$_2$ evolution: a case study of Ni(OH)$_2$/HNb$_3$O$_8$ nanocomposites, Catal. Sci. Technol. 7 (2017) 5662–5669.

[26] Y. Nakibli, P. Kalisman, L. Amirav, Less is more: The case of metal cocatalysts, J. Phys. Chem. Lett. 6 (2015) 2265–2268.

[27] Y. Ben-Shahar, F. Scotognella, I. Kriegel, L. Moretti, G. Cerullo, E. Rabani, U. Banin, Optimal metal domain size for photocatalysis with hybrid semiconductor-metal nanorods, Nat. Commun. 7 (2016) 10413.

[28] L. Amirav, F. Oba, S. Aloni, A.P. Alivisatos, Modular synthesis of a dual metal–dual semiconductor nano-heterostructure, Angew. Chem. Int. Ed. 54 (2015) 7007–7011.

[29] Y. Nakibli, Y. Mazal, Y. Dubi, M. Wächtler, L. Amirav, Size matters: cocatalyst size effect on charge transfer and photocatalytic activity, Nano Lett. 18 (2017) 357–364.

[30] K. Zhang, J. Ran, B. Zhu, H. Ju, J. Yu, L. Song, S.Z. Qiao, Nanoconfined nickel@ carbon core-shell cocatalyst promoting highly efficient visible-light photocatalytic H$_2$ production, Small 14 (2018) 1801705.

[31] Q. Xiang, J. Yu, M. Jaroniec, Synergetic effect of MoS$_2$ and graphene as cocatalysts for enhanced photocatalytic H$_2$ production activity of TiO$_2$ nanoparticles, J. Am. Chem. Soc. 134 (2012) 6575–6578.

[32] K. Chang, Z. Mei, T. Wang, Q. Kang, S. Ouyang, J. Ye, MoS$_2$/graphene cocatalyst for efficient photocatalytic H$_2$ evolution under visible light irradiation, ACS Nano. 8 (2014) 7078–7087.

[33] Y. Hou, Z. Wen, S. Cui, X. Guo, J. Chen, Constructing 2D porous graphitic C$_3$N$_4$ nanosheets/nitrogen-doped graphene/layered MoS$_2$ ternary nanojunction with enhanced photoelectrochemical activity, Adv. Mater. 25 (2013) 6291–6297.

[34] L.J. Fang, X.L. Wang, Y.H. Li, P.F. Liu, Y.L. Wang, H.D. Zeng, H.G. Yang, Nickel nanoparticles coated with graphene layers as efficient co-catalyst for photocatalytic hydrogen evolution, Appl. Catal. B: Environ. 200 (2017) 578–584.

[35] Q. Zhao, J. Sun, S. Li, C. Huang, W. Yao, W. Chen, T. Zeng, Q. Wu, Q. Xu, Single nickel atoms anchored on nitrogen-doped graphene as a highly active cocatalyst for photocatalytic H$_2$ evolution, ACS Catal. 8 (2018) 11863–11874.

[36] J. Xu, Y. Qi, L. Wang, In situ derived Ni$_2$P/Ni encapsulated in carbon/g-C$_3$N$_4$ hybrids from metal–organic frameworks/g-C$_3$N$_4$ for efficient photocatalytic hydrogen evolution, Appl. Catal. B: Environ. 246 (2019) 72–81.

[37] R. Shen, J. Xie, Y. Ding, S.-y. Liu, A. Adamski, X. Chen, X. Li, Carbon Nanotube-supported Cu$_3$P as high-efficiency and low-cost cocatalysts for exceptional semi-conductor-free photocatalytic H$_2$ Evolution, ACS Sustainable Chem. Eng. 7 (2019) 3243–3250.

[38] Y. Song, K. Xia, Y. Gong, H. Chen, L. Li, J. Yi, X. She, Z. Chen, J. Wu, H. Li, Controllable synthesized heterostructure photocatalyst Mo$_2$C@ C/2D gC$_3$N$_4$: enhanced catalytic performance for hydrogen production, Dalton Trans. 47 (2018) 14706–14712.

[39] Y.-X. Pan, J.-B. Peng, S. Xin, Y. You, Y.-L. Men, F. Zhang, M.-Y. Duan, Y. Cui, Z.-Q. Sun, J. Song, Enhanced visible-light-driven photocatalytic H$_2$ evolution from water on noble-metal-free CdS-nanoparticle-dispersed Mo$_2$C@C nanospheres, ACS Sustainable Chem. Eng. 5 (2017) 5449–5456.

[40] D. Deng, Y. Yu, X. Chen, G. Wang, L. Jin, X. Pan, J. Deng, G. Sun, X. Bao, Iron encapsulated within pod-like carbon nanotubes for oxygen reduction reaction, Angew. Chem. 125 (2013) 389–393.

[41] J. Deng, P. Ren, D. Deng, X. Bao, Enhanced electron penetration through an ultrathin graphene layer for highly efficient catalysis of the hydrogen evolution reaction, Angew. Chem. Int. Ed. 54 (2015) 2100–2104.

[42] L. Ai, J. Su, M. Wang, J. Jiang, Bamboo-structured nitrogen-doped carbon nanotube Co-encapsulating cobalt and molybdenum carbide nanoparticles: an efficient bifunctional electrocatalyst for overall water splitting, ACS Sustainable Chem. Eng. 6

(2018) 9912–9920.

[43] L. Huang, L. Ai, M. Wang, J. Jiang, S. Wang, Hierarchical MoS$_2$ nanosheets integrated Ti$_3$C$_2$ MXenes for electrocatalytic hydrogen evolution, Int. J. Hydrogen Energy 44 (2019) 965–976.

[44] Z. Niu, C. Qiu, J. Jiang, L. Ai, Hierarchical CoP-FeP branched heterostructures for highly efficient electrocatalytic water splitting, ACS Sustainable Chem. Eng. 7 (2018) 2335–2342.

[45] S. Yang, Y. Gong, J. Zhang, L. Zhan, L. Ma, Z. Fang, R. Vajtai, X. Wang, P.M. Ajayan, Exfoliated graphitic carbon nitride nanosheets as efficient catalysts for hydrogen evolution under visible light, Adv. Mater. 25 (2013) 2452–2456.

[46] L. Kong, Y. Ji, Z. Dang, J. Yan, P. Li, Y. Li, S. Liu, g-C$_3$N$_4$ loading black phosphorus quantum dot for efficient and stable photocatalytic H$_2$ generation under visible light, Adv. Funct. Mater. 28 (2018) 1800668.

[47] Q. Lin, L. Li, S. Liang, M. Liu, J. Bi, L. Wu, Efficient synthesis of monolayer carbon nitride 2D nanosheet with tunable concentration and enhanced visible-light photocatalytic activities, Appl. Catal. B: Environ. 163 (2015) 135–142.

[48] J. Xu, M. Antonietti, The performance of nanoparticulate graphitic carbon nitride as an amphiphile, J. Am. Chem. Soc. 139 (2017) 6026–6029.

[49] Y. Wang, X. Liu, J. Liu, B. Han, X. Hu, F. Yang, Z. Xu, Y. Li, S. Jia, Z. Li, Carbon quantum dot implanted graphite carbon nitride nanotubes: excellent charge separation and enhanced photocatalytic hydrogen evolution, Angew. Chem. 130 (2018) 5867–5873.

[50] G. Cai, J. Wang, X. Wu, Y. Zhan, S. Liang, Scalable one-pot synthesis of porous 0D/2D C$_3$N$_4$ nanocomposites for efficient visible-light driven photocatalytic hydrogen evolution, Appl. Surf. Sci. 459 (2018) 224–232.

[51] S. Liang, Y. Xia, S. Zhu, S. Zheng, Y. He, J. Bi, M. Liu, L. Wu, Au and Pt co-loaded g-C$_3$N$_4$ nanosheets for enhanced photocatalytic hydrogen production under visible light irradiation, Appl. Surf. Sci. 358 (2015) 304–312.

[52] G. Liu, G. Zhao, W. Zhou, Y. Liu, H. Pang, H. Zhang, D. Hao, X. Meng, P. Li, T. Kako, In situ bond modulation of graphitic carbon nitride to construct p-n homojunctions for enhanced photocatalytic hydrogen production, Adv. Funct. Mater. 26 (2016) 6822–6829.

[53] Q. Liu, T. Chen, Y. Guo, Z. Zhang, X. Fang, Ultrathin g-C$_3$N$_4$ nanosheets coupled with carbon nanodots as 2D/0D composites for efficient photocatalytic H$_2$ evolution, Appl. Catal. B: Environ. 193 (2016) 248–258.

[54] Y. Li, K. Lv, W. Ho, F. Dong, X. Wu, Y. Xia, Hybridization of rutile TiO2 (rTiO$_2$) with g-C$_3$N$_4$ quantum dots (CN QDs): an efficient visible-light-driven Z-scheme hybridized photocatalyst, Appl. Catal. B: Environ. 202 (2017) 611–619.

[55] X. Miao, X. Yue, Z. Ji, X. Shen, H. Zhou, M. Liu, K. Xu, J. Zhu, G. Zhu, L. Kong, Nitrogen-doped carbon dots decorated on g-C$_3$N$_4$/Ag$_3$PO$_4$ photocatalyst with improved visible light photocatalytic activity and mechanism insight, Appl. Catal. B: Environ. 227 (2018) 459–469.

[56] Q. Liu, L. Ai, J. Jiang, MXene-derived TiO$_2$@C/gC$_3$N$_4$ heterojunctions for highly efficient nitrogen photofixation, J. Mater. Chem. A 6 (2018) 4102–4110.

[57] X. Li, C. Zeng, J. Jiang, L. Ai, Magnetic cobalt nanoparticles embedded in hierarchically porous nitrogen-doped carbon frameworks for highly efficient and well-recyclable catalysis, J. Mater. Chem. A 4 (2016) 7476–7482.

[58] Y. Liu, H. Zhang, J. Ke, J. Zhang, W. Tian, X. Xu, X. Duan, H. Sun, M.O. Tade, S. Wang, 0D (MoS$_2$)/2D (g-C$_3$N$_4$) heterojunctions in Z-scheme for enhanced photocatalytic and electrochemical hydrogen evolution, Appl. Catal. B: Environ. 228 (2018) 64–74.

[59] Z. Pan, Y. Zheng, F. Guo, P. Niu, X. Wang, Decorating CoP and Pt nanoparticles on graphitic carbon nitride nanosheets to promote overall water splitting by conjugated polymers, ChemSusChem. 10 (2017) 87–90.

[60] Q. Zhu, B. Qiu, M. Du, M. Xing, J. Zhang, Nickel boride cocatalyst boosting efficient photocatalytic hydrogen evolution reaction, Ind. Eng. Chem. Res. 57 (2018)

8125–8130.

[61] J. Wen, J. Xie, Z. Yang, R. Shen, H. Li, X. Luo, X. Chen, X. Li, Fabricating the robust g-C$_3$N$_4$ nanosheets/carbons/NiS multiple heterojunctions for enhanced photocatalytic H$_2$ generation: an insight into the trifunctional roles of nanocarbons, ACS Sustainable Chem. Eng. 5 (2017) 2224–2236.

[62] M. Shao, Y. Shao, J. Chai, Y. Qu, M. Yang, Z. Wang, M. Yang, W.F. Ip, C.T. Kwok, X. Shi, Synergistic effect of 2D Ti$_2$C and g-C$_3$N$_4$ for efficient photocatalytic hydrogen production, J. Mater. Chem. A 5 (2017) 16748–16756.

[63] Y. Sui, J. Liu, Y. Zhang, X. Tian, W. Chen, Dispersed conductive polymer nanoparticles on graphitic carbon nitride for enhanced solar-driven hydrogen evolution from pure water, Nanoscale 5 (2013) 9150–9155.

[64] R. Ye, H. Fang, Y.-Z. Zheng, N. Li, Y. Wang, X. Tao, Fabrication of CoTiO$_3$/g-C$_3$N$_4$ hybrid photocatalysts with enhanced H$_2$ evolution: Z-scheme photocatalytic mechanism insight, ACS Appl. Mater. Interfaces 8 (2016) 13879–13889.

[65] K. Bhunia, M. Chandra, S. Khilari, D. Pradhan, Bimetallic PtAu alloy nanoparticles-integrated g-C$_3$N$_4$ hybrid as an efficient photocatalyst for water-to-hydrogen conversion, ACS Appl. Mater. Interfaces 11 (2018) 478–488.

[66] Y. Cao, D. Wang, Y. Lin, W. Liu, L. Cao, X. Liu, W. Zhang, X. Mou, S. Fang, X. Shen, Single Pt atom with highly vacant d-orbital for accelerating photocatalytic H$_2$ evolution, ACS Appl. Energy Mater. 1 (2018) 6082–6088.

[67] R. Wang, J. Yan, M. Zu, S. Yang, X. Cai, Q. Gao, Y. Fang, S. Zhang, S. Zhang, Facile synthesis of interlocking g-C$_3$N$_4$/CdS photoanode for stable photoelectrochemical hydrogen production, Electrochim. Acta 279 (2018) 74–83.

[68] S. Chen, X. Li, W. Zhou, S. Zhang, Y. Fang, Carbon-coated Cu-TiO$_2$ nanocomposite with enhanced photostability and photocatalytic activity, Appl. Surface Sci. 466 (2019) 254–261.

[69] R. Wang, S. Chen, Y.H. Ng, Q. Gao, S. Yang, S. Zhang, F. Peng, Y. Fang, S. Zhang, ZnO/CdS/PbS nanotube arrays with multi-heterojunctions for efficient visible-light-driven photoelectrochemical hydrogen evolution, Chem. Eng. J. 362 (2019) 658–666.

[70] R. Kobayashi, K. Kurihara, T. Takashima, B. Ohtani, H. Irie, A silver-inserted zinc rhodium oxide and bismuth vanadium oxide heterojunction photocatalyst for overall pure-water splitting under red light, J. Mater. Chem. A 4 (2016) 3061–3067.

[71] L. Liao, Q. Zhang, Z. Su, Z. Zhao, Y. Wang, Y. Li, X. Lu, D. Wei, G. Feng, Q. Yu, Efficient solar water-splitting using a nanocrystalline CoO photocatalyst, Nat. Nanotechnol. 9 (2014) 69.

[72] X. Meng, Y. Dong, Q. Hu, Y. Ding, Co nanoparticles decorated with nitrogen doped carbon nanotubes for boosting photocatalytic water splitting, ACS Sustainable Chem. Eng. 7 (2018) 1753–1759.

[73] R. Wang, J. Yan, M. Zu, S. Yang, X. Cai, Q. Gao, Y. Fang, S. Zhang, S. Zhang, Facile synthesis of interlocking g-C$_3$N$_4$/CdS photoanode for stable photoelectrochemical hydrogen production, Electrochimica Acta 279 (2018) 74–83.

[74] F. Shi, Z. Geng, K. Huang, Q. Liang, Y. Zhang, Y. Sun, J. Cao, S. Feng, Cobalt nanoparticles/black phosphorus nanosheets: an efficient catalyst for electrochemical oxygen evolution, Adv. Sci. 5 (2018) 1800575.

[75] Y.-J. Yuan, Z. Shen, S. Wu, Y. Su, L. Pei, Z. Ji, M. Ding, W. Bai, Y. Chen, Z.-T. Yu, Liquid exfoliation of g-C$_3$N$_4$ nanosheets to construct 2D-2D MoS$_2$/g-C$_3$N$_4$ photocatalyst for enhanced photocatalytic H$_2$ production activity, Appl. Catal. B: Environ. 246 (2019) 120–128.

[76] X. Li, X. Lv, N. Li, J. Wu, Y.-Z. Zheng, X. Tao, One-step hydrothermal synthesis of high-percentage 1T-phase MoS$_2$ quantum dots for remarkably enhanced visible-light-driven photocatalytic H$_2$ evolution, Appl. Catal. B: Environ. 243 (2019) 76–85.

[77] Y. Liu, X. Xu, J. Zhang, H. Zhang, W. Tian, X. Li, M.O. Tade, H. Sun, S. Wang, Flower-like MoS$_2$ on graphitic carbon nitride for enhanced photocatalytic and electrochemical hydrogen evolutions, Appl. Catal. B: Environ. 239 (2018) 334–344.